Nuclear Inst. and Methods in Physics Research B 434 (2018) 102–108

Contents lists available at ScienceDirect

Nuclear Inst. and Methods in Physics Research B

journal homepage: www.elsevier.com/locate/nimb

An ion-beam surface sputtering approach to the quest for lead-free metal halide perovskite for solar cells

Oluwole E. Oyewande[a,b,*], Akinwumi Akinpelu[a]

[a] Department of Physics, College of Science & Technology, Covenant University, Ota, Ogun State, Nigeria
[b] Department of Physics, Faculty of Science, University of Ibadan, Ibadan, Nigeria

ARTICLE INFO

Keywords:
Solar cells
Ion-beam surface sputtering
Perovskites
Sputter yield
Range of ions

ABSTRACT

Metal halide perovskites have been the subject of intense theoretical and experimental research in recent years, due to their huge potential over their silicon-based counterparts for tunable optoelectronic applications in high-tech device innovation. The current best perovskite for solar cell applications, with a power conversion efficiency of 22%, methylammonium lead iodide ($CH_3NH_3PbI_3$), is toxic due to the presence of lead and is therefore harmful in solar cell applications despite its low concentration in solar cells. Hence, research exploits are geared towards perovskites without lead. Unfortunately, this has taken back the gains in PCEs by about 70%, and a lot is being done for improvement. In this paper, a new approach to these studies is introduced by performing Monte Carlo simulations of ion-beam sputtering of lead and tin perovskites, as well as other promising candidate materials, in order to throw some light on their potentials for higher efficiencies in photovoltaic applications. The sputtering characteristics of six promising perovskites, including lead perovskite and lead-substituted perovskites, were compared. The results showed a remarkable exhibition of similar sputtering characteristics of linear projected ion range for Pb and Sn, with a maximum sputter yield around 78° ion incidence. The results also indicated a correspondence between the sputtering characteristics and PCE.

1. Introduction

Lead halide perovskites have huge potential for applications in solution-based photovoltaics (e.g. solar cells), with greater power conversion efficiencies (PCEs) than silicon-based photovoltaics [1]. However, they suffer a large setback in these applications due to the toxicity of lead and its solubility in water. There has therefore been an intense research interest with promising results in recent years on less toxic metal replacements [2–6]. One advantage of perovskite-based photovoltaics over their silicon-based counterparts is their low-cost fabrication due to the possibility of producing them in a variety of ways, including the use of vacuum techniques [7].

A vacuum processing and fabrication technique is ion-beam sputtering of materials, which is an area of current intensive research as a cost-effective method of surface analysis, processing and fabrication of self-organized nanostructures for optoelectronic applications [8–14]. A new radio-frequency-sputtering method of production of lead-iodide perovskite was proposed in Ref. [15]. This comprises of a deposition of thin films of lead sulphide, their conversion to perovskites by placement in an iodine atmosphere, and subsequent immersion into a solution of methylammonium (i.e. solution based). Whereas in Ref. [16], a non-solution based method of perovskite film fabrication by sputtering was proposed. They confirmed that sputter-processed perovskite films showed similar characteristics as their solution-processed counterparts and produced perovskite solar cells with higher PCEs.

In a sputtering process, an incoming ion collides with an atom of the target material and sets off secondary collision cascades leading to kinetic and thermal agitations of the target atoms. Noble gas ions are commonly used in sputtering experiments because the use of other ions (e.g. N_2^+, O_2^+) can cause local changes in surface composition, hence, unusual morphology [17–26]. By virtue of the nature of the sputtering process and the need for kinetic details within the earliest impact times, molecular dynamics simulation can be exploited. However, surface topographies of interest develop at much larger timescales beyond the feasibility of molecular dynamics. In such time regimes, statistical collisional data are acquired and exploited in Monte Carlo simulation approaches. A number of enquiries have taken this approach, focusing on specific sputtering conditions (e.g. [27–30]).

A Monte Carlo simulation suite developed by Ziegler and Biersack [31–34], Stopping and Range of Ions in Matter (SRIM), and its more extended counterpart, TRansport of Ions in Matter (TRIM), which includes SRIM and calculation of some sputtering parameters with Monte

* Corresponding author at: Department of Physics, Faculty of Science, University of Ibadan, Ibadan, Nigeria.
E-mail addresses: oluwole.oyewande@covenantuniversity.edu.ng (O.E. Oyewande), akinwumi.akinpelu@covenantuniversity.edu.ng (A. Akinpelu).

https://doi.org/10.1016/j.nimb.2018.08.041
Received 21 June 2018; Received in revised form 25 August 2018; Accepted 26 August 2018
Available online 31 August 2018
0168-583X/

Carlo (MC) techniques, are versatile tools in this regard [34]. Signatures of the ion-target interaction are the collision cascade parameters and sputter yield. These can be drastically changed by minute changes in the target composition. It is therefore of interest to know the effect of lead replacement on the sputter characteristics of metal halide perovskites. By extension, it is of interest to know whether sputter characteristics, or changes in them as some element of perovskites is changed, has a correspondence with the PCE of the perovskites.

Although, ion-beam surface sputtering (IBSS) has been used for decades as a tool for the unravelling of the composition of materials, hence their intrinsic physical differences, via secondary ion mass spectrometry, this IBSS approach has never been used to investigate the physical factors responsible for differences in optoelectronic properties of structurally similar materials (e.g. perovskites in photovoltaic applications). This is the approach we now take here via MC simulations.

The most suitable material, among perovskites, for a case study in this regard is tin perovskite, $CH_3NH_3SnI_3$, which is a 3D-structure metal halide perovskite with similar characteristics as $CH_3NH_3PbI_3$ (also 3D) but with a reportedly much lower PCE of 6.4% [2]. It, nonetheless, has the highest PCE among all the lead-substituted perovskites [7]. However, Pb, Sn or Ge are good occupants of the B-site for a stable perovskite ABX_3 structure, where the monovalent organic cation (e.g. methylammonium, $CH_3NH_3^+$) occupying the position A, the halide counter-ion (e.g. iodine, I^-) occupying the X-site, or even the metallic occupant of the B-site, of the perovskite structure can be changed [e.g. the 0D-Dimer $Cs_3Bi_2I_9$, 2D $Rb_3Sb_2I_9$, or 2D $(CH_3(CH_2)_3NH_3)_2CuBr_4$]to tune the properties of the perovskite.

In this paper, we studied the range and sputter yield of ions in $CH_3NH_3PbI_3$ (lead), $CH_3NH_3SnI_3$ (tin), $CH_3NH_3GeI_3$, Cs3Bi2I9, $Rb_3Sb_2I_9$ and $(CH_3(CH_2)_3NH_3)_2CuBr_4$ perovskites, for different ion energies and incidence angles, by Monte Carlo simulations, using SRIM and TRIM. We used ions of inert gases Ne and Ar in the sputtering of these perovskites. The rest of the paper is organized as follows. In the next section we elaborated on the methods used to obtain our results. For reproducibility, we provided details of the simulation set-up. We presented and discussed our results in Section 3, and provided our conclusions in Section 4.

2. Methodology

In this section we provided the specific details of our simulation. Details of the theoretical background for the calculations and simulation algorithms embedded in the TRIM and SRIM packages are discussed in the papers by Ziegler and Biersack [31–34]. SRIM was used to perform MC simulations of the range of inert gas ions Ne^+ and Ar^+, with energies varied from 1 keV to 10 keV, at normal incidence on the targets. Ion energies in sputtering experiments, in general, fall within 10 keV. The ones that do not fall within the range are low-energy sputtering experiments with ion energy around 500 eV. Hence, the chosen range is relevant to typical ion energies. The targets were lead perovskite $CH_3NH_3PbI_3$ and tin perovskite $CH_3NH_3SnI_3$. While TRIM was used to perform MC simulations for the number of each component of the perovskites yielded as a result of bombardment of the perovskite by an incident ion, for varied incidence angles from 0° to 89°, and for ion energies 1 keV and 5 keV.

In TRIM set-up, perovskite wafer thickness of 35 nm was used. For both SRIM and TRIM, the lead, tin and germanium perovskites were built from their composites in the stoichiometric ratio 1:3:1:3:1:3 for C, H, N, H, Pb/Sn/Ge and I, respectively. Densities 4.16 g/cm^3 [35] and 3.51 g/cm^3 [36] were used, in the calculations, for the lead and tin perovskites, respectively. Experimental densities were unavailable for germanium perovskite and the remaining perovskites. Hence, the densities were calculated, using TRIM, instead. However, calculated densities for lead and tin perovskites were 2.49 g/cm^3 and 2.15 g/cm^3, respectively, which underestimated the actual (experimental) values by roughly 40%.

Therefore, for Ge perovskite a density of 3.32 g/cm^3 (i.e. with a correction factor of 5/3 of the calculated density) was used instead of the calculated density of 1.99 g/cm^3. The $(CH_3(CH_2)_3NH_3)_2CuBr_4$ was built from its composites in the ratio 2:6:6:12:2:6:1:4 for C, H, C, H, N, H, Cu and Br, respectively, and a density of 1.87 g/cm^3 was used instead of the calculated density of 1.12 g/cm^3. Both $Rb_3Sb_2I_9$ and $Cs_3Bi_2I_9$ were composed in the stoichiometric ratio 3:2:9 for Rb/Cs, Sb/Bi and I, respectively, with densities of 7.43 g/cm^3 and 8.30 g/cm^3, instead of the calculated densities of 4.46 g/cm^3 and 4.98 g/cm^3, respectively. An amount of 1000 ions was used for each simulation to allow the simulation to run for a reasonably long time. “Monolayer Collision Step/Surface Sputtering” was performed to calculate the sputter-yield in the TRIM set-up, while detailed calculation with full damage cascade was performed to calculate the projected range in the SRIM set-up.

3. Results and discussion

The results of our simulations are presented and discussed in this section. Similar trends were observed for the two ions (Ne^+ and Ar^+), though lower values of Ar^+ ion range, and higher values of Ar^+ sputter yield, than the corresponding values for Ne^+ were found. The simulations were started with the lead (Pb) perovskite (Figs. 1–7) and its most promising substitute, tin(Sn) perovskite, before performing those for the other possible substitutes which have much lower PCEs (Figs. 8–11). Fig. 1 shows the results of the projected range of the ions

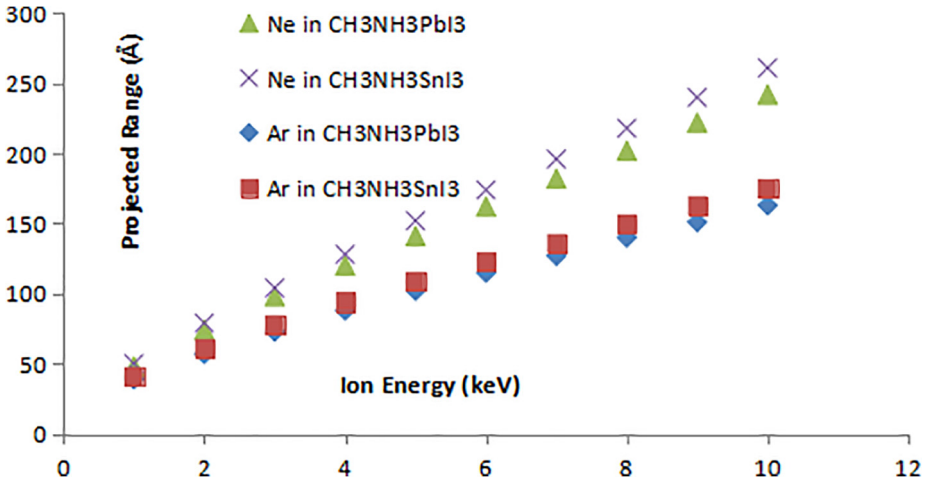

Fig. 1. Projected range of Ne^+ and Ar^+ ion in lead- and tin-perovskite targets for different ion energies from 1 keV to 10 keV.

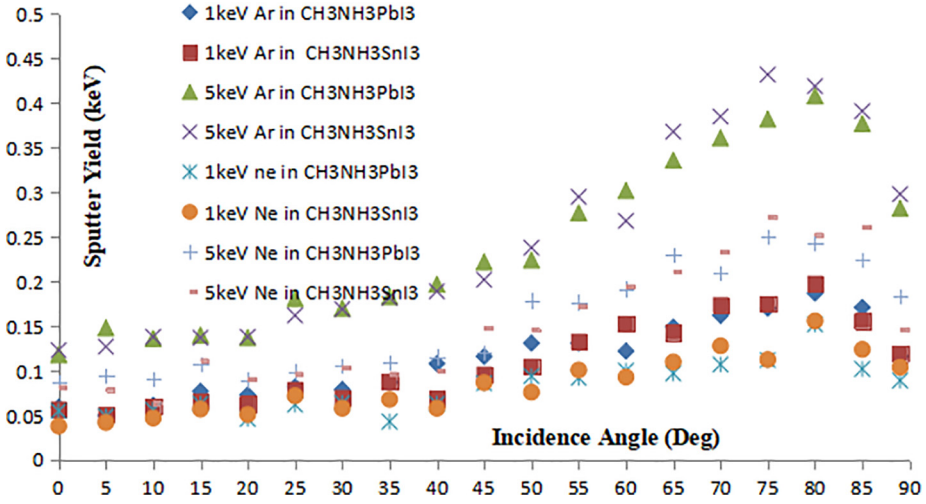

Fig. 2. Sputter yield of C (atoms/ion) for the ejection of C atoms from Ar^+ and Ne^+ bombardment of the perovskites at different angles of incidence, for ion energy of 1 keV and 5 keV.

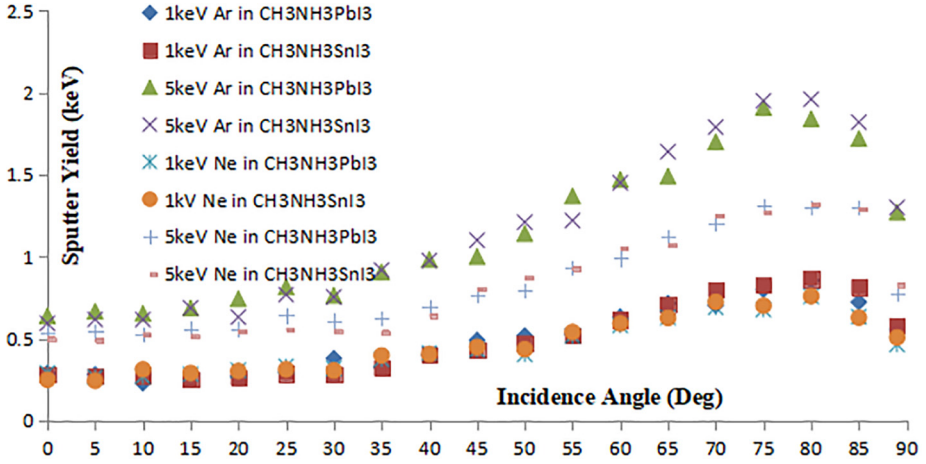

Fig. 3. Sputter yield of H^1 (atoms/ion) for the sputter erosion of H atoms of the methyl molecule from Ar^+ and Ne^+ bombardment of the perovskites at different angles of incidence, for ion energy of 1 keV and 5 keV.

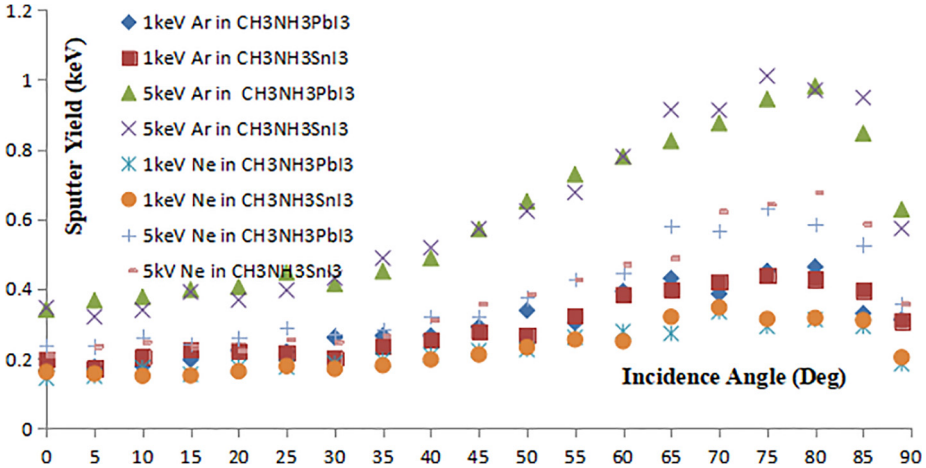

Fig. 4. Sputter yield of N (atoms/ion) for the erosion of N atoms from Ar^+ and Ne^+ bombardment of the perovskites at different angles of incidence, for ion energy of 1 keV and 5 keV.

in the two perovskites for different ion energies of 1 keV to 10 keV. The values of the linear range of the ions in the two different perovskites were close, especially for sputtering with Ar^+. These indicated that the two materials were remarkably similar as regards their stopping power to energetic particle irradiation. They reflected the choice of Sn as a good substitute for Pb in the solar cell perovskite materials.

Sputter yield results are presented as follows, one for each element in the perovskite, namely, C, H^1 (H of the methyl molecule), N, H^2 (H of the

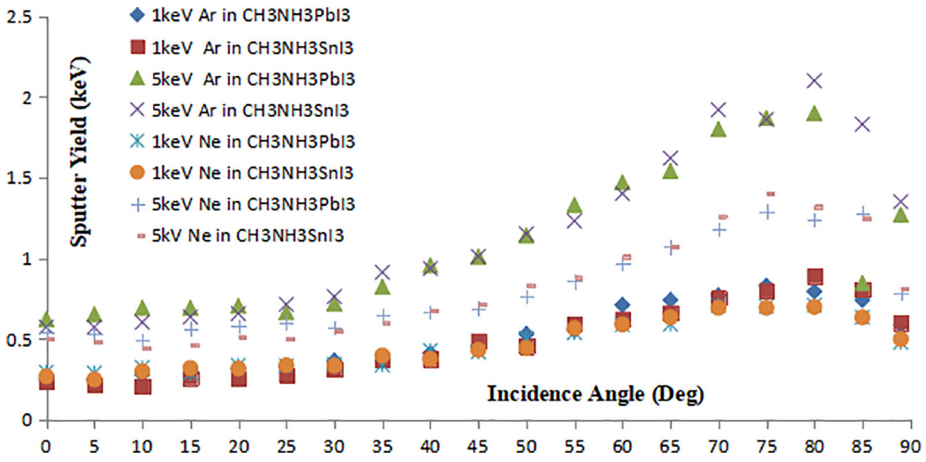

Fig. 5. Sputter yield of H^2 (atoms/ion) for the ejection of H atoms of the ammonium molecule from Ar^+ and Ne^+ bombardment of the perovskites at different angles of incidence, for ion energy of 1 keV and 5 keV.

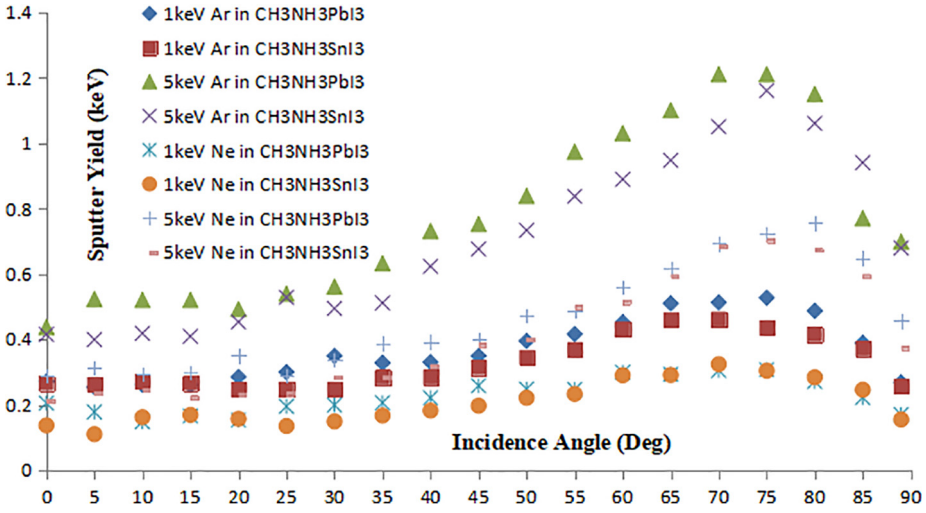

Fig. 6. Sputter yield of Pb/Sn (atoms/ion) for the erosion of Pb/Sn atoms from Ar^+ and Ne^+ bombardment of the perovskites at different angles of incidence, for ion energy of 1 keV and 5 keV.

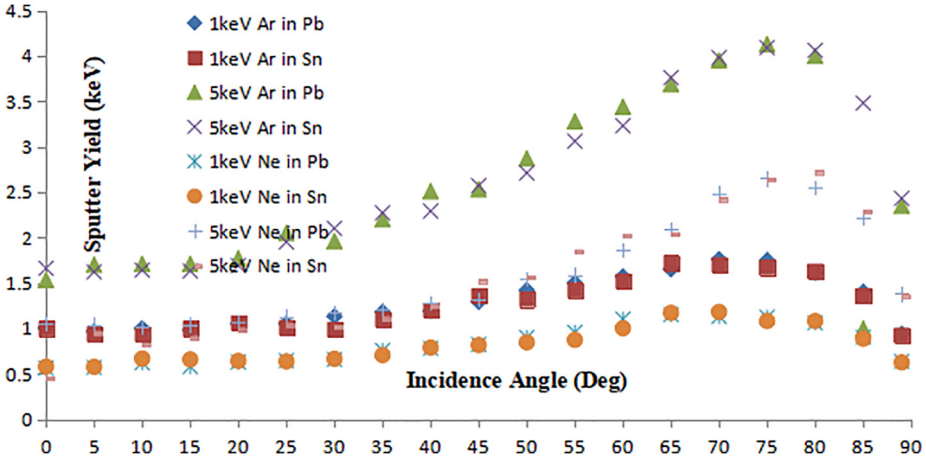

Fig. 7. Sputter yield of I (atoms/ion) for the erosion of I atoms from Ar^+ and Ne^+ bombardment of the perovskites at different angles of incidence, for ion energy of 1 keV and 5 keV.

ammonium molecule), Pb/Sn, I. Fig. 2 shows the result for the number of C atoms ejected per incident Ar^+, and Ne^+, ion on the lead and tin perovskites at different angles of incidence varied from 0° to 89°, for ion energy of 1 keV and 5 keV. The same variables apply to Figs. 3–7, but for the other elements, respectively (see the list above). For all results the yield was higher for higher ion energy, and generally increased with increasing θ (except for some fluctuations) up to a maximum yield which occurred between 70° and 82°, but mostly around 78°.

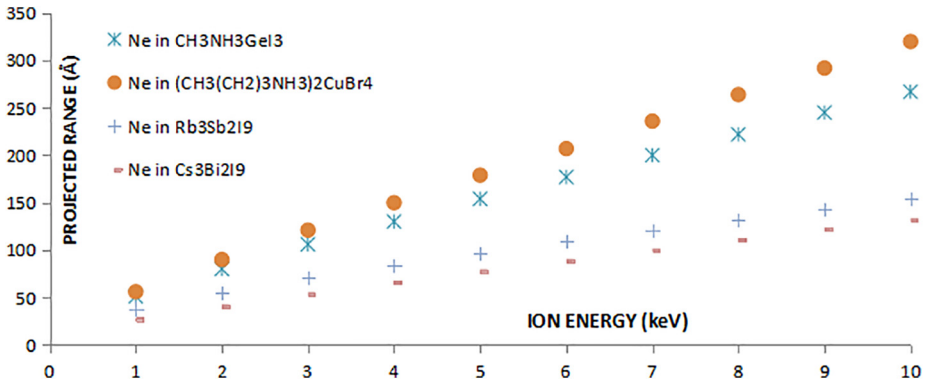

Fig. 8. Projected range of Ne^+ in each of the remaining perovskites for different ion energies from 1 keV to 10 keV.

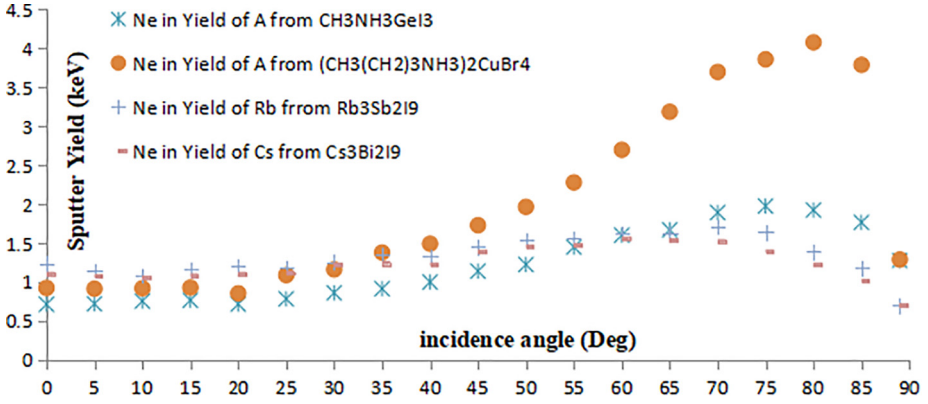

Fig. 9. Sputter yield (atoms/ion) for the erosion of A cations from Ne^+ bombardment of the remaining perovskites at different angles of incidence, and ion energy 1 keV.

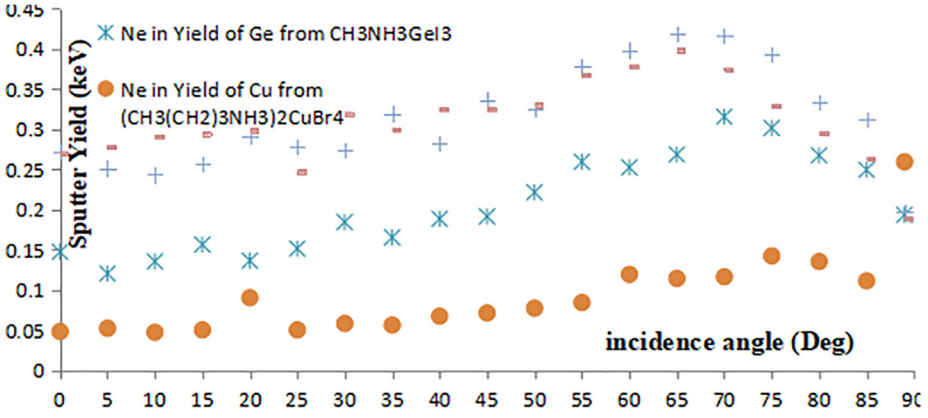

Fig. 10. Sputter yield (atoms/ion) for the erosion of B cations from Ne^+ bombardment of the remaining perovskites at different angles of incidence, and ion energy 1 keV.

The yield of C atoms was from 0.03 to 0.20 (Fig. 2) for 1 keV ion sputtering of Pb and Sn, whereas for the higher ion energy of 5 keV, it was from 0.08 to 0.43. Fig. 3 shows the yield of H^1 atoms as ranging from 0.24 to 0.86 for 1 keV ion energy, and from 0.50 to 1.95 for 5 keV ion. The yield ranges of 1 keV and 5 keV ion energy, respectively, are 0.16–0.46 and 0.21–1.01 (Fig. 4); 0.24–0.89 and 0.50–2.10 (Fig. 5); 0.13–0.53 and 0.21–1.21 (Fig. 6); 0.45–1.76 and 1.05–4.09 (Fig. 7); for the erosion of N, H^2, Pb/Sn, and I, respectively.

The C atom maximum yield is the lowest (Fig. 2), followed by N atom (Fig. 4), Pb/Sn atom (Fig. 6), H^1 atom (Fig. 3), H^2 atom (Fig. 5), and the highest yield is that of the I atom (Fig. 7), for the two ion energies. Note that in Fig. 6 only two sets of data were available for each (Pb or Sn) since Pb is not available in tin perovskite or vice versa.

The values of the two H atom yields are close, with the yield of H^1 being slightly lower.

Since the results for Ar^+ and Ne^+ over the range of incidence angles follow a similar trend, likewise the results for 1 keV and 5 keV ion energies, only the results for Ne^+ and for 1 keV ion energy are, henceforth, presented. The results of Ne ion-beam sputtering of the remaining metal halide perovskites are as follows.

Fig. 8 is a presentation of the simulation results of the range of Ne ion in each of the remaining perovskites, namely: $CH_3NH_3GeI_3$, $Cs_3Bi_2I_9$, $Rb_3Sb_2I_9$ and $(CH_3(CH_2)_3NH_3)_2CuBr_4$. The values of the range increase vis-a-vis power conversion efficiencies of the perovskites (see Ref. [7] for reported PCEs). The only exception is $(CH_3(CH_2)_3NH_3)_2CuBr_4$, for which a PCE of 0.63% had been reported,

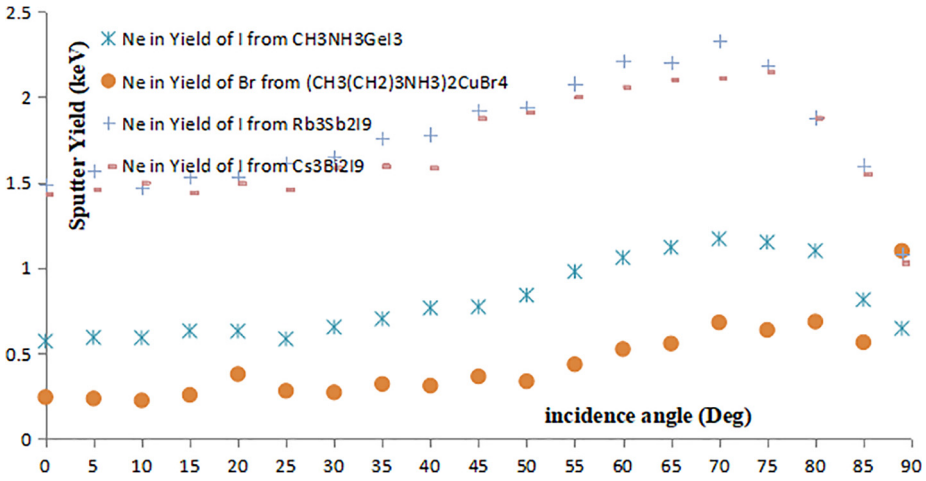

Fig.11. Sputter yield (atoms/ion) for the erosion of X cations from Ne^+ bombardment of each of the remaining perovskites at different angles of incidence, and ion energy 1 keV.

whose range curve should be between those of $Rb_3Sb_2I_9$ and $CH_3NH_3GeI_3$ which were reported to have PCEs of 0.66% and 0.20%, respectively. Therefore, this figure indicates a correspondence between projected range values and PCE, for perovskites that have the same halide content.

The results of sputter yield versus incidence angle for the remaining perovskites are presented in Figs. 9–11. For uniformity and conciseness, detailed sputter yield results for each constituent of the perovskites were not presented as done for lead and tin perovskites above, since the Cu and Sb perovskites have different cation and halide ion compositions. Hence, sputter yield results of the cation occupants of the A-site, metallic occupant of the B-site, and the halide ion occupant of the X-site were presented instead.

Fig. 10 displayed a similar trend as Fig. 9, from the critical angle of ~78° for maximum yield onward, and therefore supports our earlier inference of correspondence between sputtering characteristics and PCEs. But this appears the other way round in Figs. 9–11 (though 11 is a little vague for the Bi and Sb perovskites), where the yield appears to decrease with increasing efficiency except, again, for the Cu perovskite.

Thus, these results provide an indication of a correspondence (direct or inverse) between the sputter characteristics and PCE.

4. Conclusion

We performed Monte Carlo simulations of the ion sputtering of methylammonium lead iodide (lead perovskite) and its lead-substituted counterparts, methylammonium tin iodide (tin perovskite) and four other promising perovskites as a new perspective for understanding and improving upon the desired physical properties of less toxic perovskite materials that are based on the possible substitutes for lead.

Currently, the perovskites of these substitutes have a much lower PCE than lead perovskite. In our studies, reported in this paper, we found the sputtering results of lead perovskite and its best substitute so far, tin perovskite, to be very similar. In fact, so similar as to serve as another reason why the quest to improve upon the properties of tin perovskites, towards the desired better PCE in tin halide perovskite based solar cell applications, should not be abandoned despite its current very poor PCE. The results also indicated a correspondence between sputtering characteristics and PCEs.

Acknowledgement

The authors thank the Covenant University Centre for Research, Innovation and Discovery (CUCRID) for research support.

References

[1] Photovoltaics, National Renewable Energy Laboratory, 2018.
[2] N. Noel, S. Stranks, A. Abate, C. Wehrenfennig, S. Guamera, A. Haghighirad, A. Sadhanala, G. Eperon, S. Pathak, M. Johnston, A. Pertozza, L. Herz, H. Snaith, Energy Environ. Sci. 7 (2014) 3061.
[3] T. Krishnamoorthy, H. Ding, C. Yan, W. Leong, T. Baikie, Z. Zhang, M. Sherburne, S. Li, M.N. Asta, S. Mhaisalkar, J. Mater. Chem. A3 (2015) 23829.
[4] X. Cui, K. Jiang, J. Huang, Q. Zhang, M. Su, L. Yang, Y.-L. Song, X.-Q. Zhou, Synth 209 (2015) 247.
[5] B. Park, B. Philippe, X. Zhang, H. Rensmo, G. Boschloo, E. Johansson, Adv. Mater 27 (2015) 6806.
[6] P. Harikesh, H. Mulmudi, B. Ghosh, T. Goh, Y. Teng, K. Thirumal, M. Lockrey, K. Weber, T. Koh, S. Li, S. Mhaisalkar, N. Mathews, Chem. Mater 28 (2016) 7496.
[7] S. Hoefler, G. Trimmel, T. Rath, Progress on lead-free metal halide perovskites for photovoltaic applications: a review, Monatsh Chem. 148 (2017) 795.
[8] E. Oyewande, Modelling and simulation of surface morphology driven by ion bombardment, Ph.D Thesis, Goettingen, 2006.
[9] M.O.-G. Javier, L. Vazquez, M. Castro, R. Gago, A. Redondo-Cubero, A. Moreno-Barrado, R. Cuerno, Self-organized nano patterning of silicon surfaces by ion beam sputtering, Materials Science and Engineering B 86 (2014) 1–14.
[10] O. Oyewande, A. Hartmann, R. Kree, Phys. Rev. B 71 (2005) 195405.
[11] E. Oyewande, R. Kree, A. Hartmann, Morphological regions and oblique-incidence dot formation in a model of surface sputtering, Phys. Rev B. 75 (2006) 115434.
[12] E. Oyewande, R. Kree, A. Hartmann, Numerical analysis of quantum dots on off-normal incidence ion sputtered surfaces, Phys. Rev. B 75 (2007) 155325.
[13] R. Kree, A. Hartmann, Geyer, M. Kolbel, Long-time effects in a simulation model of sputter erosion, Phys. Rev. B 65 (2002) 193403.
[14] O. Oyewande, A unified spatio-temporal framework of the Cuerno-Barabasi stochastic continuum model of surface sputtering, Commun. Theor. Phys. 58 (2012) 165–170.
[15] José Maria Clemente da Silva Filho, Viktor A. Ermakov, Francisco Chagas Marques, Perovskite thin film synthesised from sputtered lead sulphide, Sci. Rep. 8 (2018) 1563.
[16] I. Raifuku, Y. Ishikawa, T. Bourgeteau, Y. Bonnassieux, P. Cabarrocas, Y. Uraoka, Fabrication of perovskite solar cells using sputter-processed CH3NH3PbI3 films, Appl. Phys. Expr. 10 (2017) 094101.
[17] M.O.-G. Javier, V.Z. Luis, C. Mario, L.G. Raú, S.R.-C. Andre, M.-B. Ana, C. Rodolfo, Self-organized nanopatterning of silicon surfaces by ion beam sputtering. Materials Science and Engineering R, Nucl. Inst. Meth. Phys. Res. B 86 (2014) 1–44.
[18] M. Castro, R. Gago, et al., Nucl. Instrum. Meth. Phys. Res. B 86 (2012) 214107.
[19] C. Madi, B. Davidovitch, H. George, S. Norris, M. Brenner, M. Aziz, Phys. Rev. Lett. 101 (2008) 246102.
[20] C. Madi, H. George, M. Aziz, J. Phys.: Condens. Matter. 21 (2009) 224010.
[21] M. Feix, A. Hartmann, R. Kree, J. Munoz-Garcia, R. Cuerno, Phys. Rev. B 71 (2005) 12540.
[22] W. Moeller, TRI3DYN, Collisional computer simulation of the dynamic evolution of 3-dimensional nanostructures under ion irradiation, Nucl. Instrum. Meth. Phys. Res. B 322 (2014) 23–33.
[23] H. Hofsass, O. Bobes, K. Zhang. p. 386.
[24] S. Macko, F. Frost, B. Ziberi, D. Förster, T. Michely, Nanotechnol. 21 (2010) 085301.
[25] E. Anzenberg, J. Perkinson, C. Madi, M. Aziz, K.J. Ludwig, Phys. Rev. B 86 (2012) 245412.
[26] M. Teichmann, J. Lorbeer, B. Ziberi, F. Frost, B. Rauschenbach, New J. Phys. 15 (2013) 103029.
[27] H. Hofsass, K. Zhang, A. Mutzke, Simulation of ion beam sputtering with SDTrimSP, TRIDYN and SRIM, Appl. Surf. Sci. 310 (2014) 134–141.

[28] W. Moeller, TRI3DYN, Collisional computer simulation of the dynamic evolution of 3-dimensional nanostructures under ion irradiation, Nucl. Istrum. Meth. Phys. Res. B 412 (2014) 23–33.
[29] Y. Shulga, Sputter yield of rippled surfaces: a simulation study, Nucl. Instrum. Meth. Phys. Res. B 412 (2017) 207–213.
[30] J. Ziegler, J. Biersack, U. Litmark, Stopping and Range of Ions in Solids, Pergamon, New York, 1985.
[31] J. Ziegler, J. Biersack, "TRIM," SRIM.
[32] J. Ziegler, M. Ziegler, J. Biersack, The stopping and range of ions in matter, Nucl. Instrum. Meth. Phys. Res. B 268 (2010) 1818–1823.
[33] S. Martinie, T. Saad-Saoud, S. Moindjie, D. Munteanu, J. Autran, Behavioral modeling of SRIM tables for numerical simulation, Nucl. Instrum. Meth. Phys. Res. B 322 (2014) 2–6.
[34] W. Wilson, L. Haggmark, J. Biersack, Calculations of nuclear stopping, ranges, and straggling in the low-energy region, Phys. Rev. B 15 (1997) 2458.
[35] J. Huang, K. Jiang, X. Cui, Q. Zhang, M. Gao, M. Su, L. Yang, Direct conversion of of CH3NH3PbI3 from electrodeposited PbO for highly efficient planar perovskite solar cells, Sci. Rep. 5 (2015) 15889.
[36] C. Kim, T. Huan, S. Krishnan, A. Ramprasad, A hybrid organic inorganic perovskite dataset, Sci. Data 4 (2017) 170057.